A NEW 1-D COLOUR MODEL AND ITS APPLICATION TO IMAGE FILTERING

Frederic Garcia[⋆†] *Djamila Aouada*[⋆] *Bruno Mirbach*[†] *Björn Ottersten*[⋆]

[†]Advanced Engineering Department, IEE S.A.
{frederic.garcia, bruno.mirbach}@iee.lu

[⋆]Interdisciplinary Centre for Security, Reliability and Trust,
University of Luxembourg
{djamila.aouada, bjorn.ottersten}@uni.lu

ABSTRACT

This paper introduces a new 1-D model to encode coloured images for an efficient subsequent processing. This representation is equivalent to, but more compact than, the 3-D HCL conical representation. It consists in gathering all the hue, chroma and luminance information in one component, namely, the cumulative spiral angle, where the spirals in question are defined as a sampling of the solid HCL cone. We use the proposed model for joint bilateral upsampling of low-resolution depth maps. The results show that, in addition to preserving the perceptual properties of the HCL colour representation, using the proposed model leads to a solution that is more accurate than when using grayscale images.

I. INTRODUCTION

Many image processing algorithms consider grayscale images as input data. Although the results can be more accurate when considering the full colour information, most systems are restricted by processing time and memory constraints, mainly if real-time is a requirement. A grayscale image is defined as a linear combination of the red, green, and blue channels in the RGB space. This combination leads to a non-unique representation of the true colours, which may cause serious artefacts such as missing features, bad image matching, or non-detection of salient points. As a result, a more accurate processing of images requires calling upon their true colours, and using three components. Indeed, most algorithms have their definitions extended to three channels such as bilateral filtering [1], [2], image sharpening and denoising [3], image enhancement [4], etc. Paris et al. tested several alternatives on a colour image [2]. They first filtered an RGB image as three independent channels. Despite a correlation between the three channels, they showed that edges may be smoothed in one channel while they are preserved in another channel. This consequently induces incoherent results between channels. They then tested reducing these inconsistencies, that result in bleeding effect, by processing the R, G, and B channels altogether. The downside of this approach was, however, a longer computational time required for processing. The same authors tested filtering images in the CIE-Lab space, which is known to be perceptually meaningful. Indeed, this solved the colour-bleeding problem but not the demanding computation time. In this paper, we propose to reduce the complexity of processing 3 channels by compactly storing the same information in only one channel. To that end, we exploit the geometrical structure of 3-D conical colour spaces and show how to accurately define one parameter to represent the solid HCL conical colour space [5]. We equip this representation with an associated colour similarity measure inspired from the cylindrical distance used for cylindrical and conic colour spaces such as HSV/HSL [5], [6], [7]. The proposed colour model represents a novel colour ordering that might be useful in the context of colour morphology [8]. Indeed, morphological colour operators, i.e., morphological filters such as opening and closing or morphological centre, can be adapted to the proposed colour ordering for further image processing such as image denoising. We note that our work is not only related to data compression from 3-D to 1-D [9] but deals also with a colour codification for an efficient subsequent processing.

The organization of the paper is as follows: In Section 2, we refer to our prior work on the reduction of a 3-D colour space to 2-D. We then go one step further and propose in Section 3 to reduce the dimensionality to one, where the entire cone space is approximated by a single parameter. In Section 4, we directly use the proposed 1-D colour model for low-resolution depth map bilateral filtering. We present, in Section 5, the experimental results and conclude in Section 6.

II. PRIOR WORK: FROM 3-D TO 2-D

We proposed in [10] to describe the colour information contained in the HCL (hue, chroma, luminance) conic space, shown in Fig. 1(a), by approximating the cone using two parameters, θ and l, instead of using the three coordinates (h, c, l). Our key idea is to approximate the chromaticity disk with a spiral, as shown in Fig. 1(b). To that end, we choose to use the *Archimedean* spiral [11] whose radial distance

is defined as $r(\theta) := \mathsf{a} \cdot \theta$, where $\mathsf{a} = \frac{1}{2\pi \mathsf{K}}$ is a constant defining the distance between successive turns, and θ is the polar angle of the spiral, such that $\theta \in [0, 2\pi\mathsf{K}]$, K being the total number of turns. We then save the luminance value l,

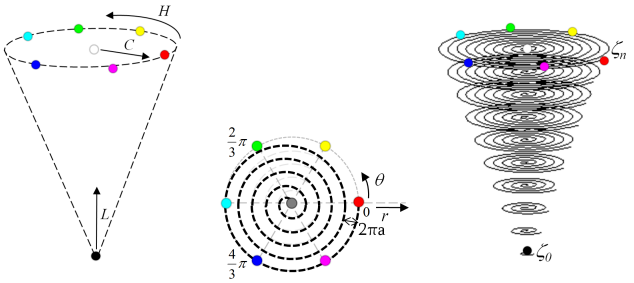

(a) (b) (c)

Fig. 1. (a) HCL colour space model. (b) Chromaticity disk approximation with a spiral. (c) Approximation of the HCL cone by a set of spirals.

and rewrite h and c as functions of a new variable θ such that:

$$\theta = h - 2\pi \,\text{round}\left(\mathsf{K} \cdot c - \frac{h}{2\pi}\right). \tag{1}$$

In what follows, our next objective is to define one spiral for the approximation of the whole HCL solid cone.

III. PROPOSED 1-D COLOUR MODEL

In order to include the luminance parameter in the definition of the spiral model in (1), we propose to uniformly sample the luminance axis into $(\mathsf{K_L} + 1)$ values l_n. We thus have:

$$l_n = \frac{n}{\mathsf{K_L}}, \tag{2}$$

where $n \in \{0, 1, \cdots, \mathsf{K_L}\}$. At each luminance level l_n, we define a spiral of radius $r(\theta_n) = \mathsf{a} \cdot \theta_n$, with $\theta_n \in [0, 2\pi n]$. In other words, for larger sections of the cone, we impose a larger number of spiral turns, as shown in Fig. 1(c). In order to keep a single parametrization of all the $\mathsf{K_L}$ spirals, we need to relate all of them to the same parameter. To that end, for a point on the spiral at the level l_n, we introduce the *cumulative angle* (CA) ζ as:

$$\zeta = \zeta_{n-1} + \theta, \tag{3}$$

with

$$\zeta_{n-1} = \sum_{i=0}^{n-1} 2\pi \cdot i = n(n-1) \cdot \pi. \tag{4}$$

We note that ζ_{n-1} is the CA of the spirals at level l_{n-1}. The colour model proposed in (3), that we call CA model, reduces the HCL space to a 1-D representation by a single parameter ζ. We also notice that the CA model is reversible from and to the original HCL space and consequently to all colour spaces that can be converted from and to HCL, such as RGB. To do so, one simply needs to follow two steps; first to retrieve l or its approximation l_n, and second find the pair (h, c) at the corresponding level. By definition, we find that:

$$\zeta_{n-1} \leq \zeta < \zeta_n \implies l \approx l_n \text{ and } \theta = \zeta - \zeta_{n-1}. \tag{5}$$

By solving the two inequalities in (5), we find an analytical expression for n avoiding a search among the intervals $[\zeta_{n-1}, \zeta_n[$. As an intermediary step, we get:

$$\left(\frac{-1 + \sqrt{1 + \frac{4}{\pi}\zeta}}{2}\right) < n \leq \left(\frac{1 + \sqrt{1 + \frac{4}{\pi}\zeta}}{2}\right). \tag{6}$$

Given that $n \in \mathbb{N}$, we find:

$$n = \left\lfloor \frac{1}{2}\sqrt{1 + \frac{4}{\pi}\zeta} + \frac{1}{2} \right\rfloor, \tag{7}$$

and from (2) we obtain l_n. To obtain the pair (h, c), we simply need to follow the same steps presented in [10] using the θ angle from (3). We finally get the following result:

$$\begin{cases} h \equiv \zeta \mod 2\pi, \\ c = \frac{1}{2\pi\mathsf{K}} \left\lfloor \frac{1}{2}\sqrt{1 + \frac{4}{\pi}\zeta} + \frac{1}{2} \right\rfloor \left\lfloor \frac{1}{2}\sqrt{1 + \frac{4}{\pi}\zeta} - \frac{1}{2} \right\rfloor, \\ l = \frac{1}{\mathsf{K_L}} \cdot \left\lfloor \frac{1}{2}\sqrt{1 + \frac{4}{\pi}\zeta} + \frac{1}{2} \right\rfloor. \end{cases} \tag{8}$$

With equations (8) at hand, we fully defined a bijective transformation from (h, c, l) to ζ. This means that the CA representation encodes in one channel all the information contained in three channels with an easy way to back-transform. Such a model gives the possibility to apply the same algorithms used with grayscale images on full color information, but without extending the algorithms to 3 channels. We illustrate this by using the CA model for depth map filtering.

IV. APPLICATION TO DEPTH MAP FILTERING

We consider as an application example the joint bilateral upsampling filter (JBU) [1]. The JBU enhances a low-resolution depth map $\mathbf{R}$ acquired by a range camera to the same spatial resolution of a 2-D image $\mathbf{I}$ acquired from the same point of view. This multilateral filter has two weighing terms, often chosen to be Gaussian functions. The first one is spatial, $G_{\mathsf{s}}(\cdot)$, with a standard deviation σ_{s}, and the second one $G_{\mathsf{r}}(\cdot)$, operating on the 2-D images $\mathbf{I}$, with a standard deviation σ_{r}. The output of the JBU filter is defined as:

$$\mathbf{J}(\mathbf{p}) = \frac{\sum_{\mathbf{q} \in N(\mathbf{p})} G_{\mathsf{s}}\left(\|\mathbf{p} - \mathbf{q}\|\right) \cdot G_{\mathsf{r}}\left(d\left(\mathbf{I}(\mathbf{p}), \mathbf{I}(\mathbf{q})\right)\right) \cdot \mathbf{R}(\mathbf{q})}{\sum_{\mathbf{q} \in N(\mathbf{p})} G_{\mathsf{s}}(\|\mathbf{p} - \mathbf{q}\|) \cdot G_{\mathsf{r}}\left(d\left(\mathbf{I}(\mathbf{p}), \mathbf{I}(\mathbf{q})\right)\right)},$$

where $N(\mathbf{p})$ is the neighbourhood at the pixel location $\mathbf{p} = (i, j)^T$, where i corresponds to rows and j corresponds to columns. $d\left(\mathbf{I}(\mathbf{p}), \mathbf{I}(\mathbf{q})\right)$ is a distance between two image intensity values, $\mathbf{I}(\mathbf{p})$ and $\mathbf{I}(\mathbf{q})$. In the standard case of grayscale images, this distance is Euclidean. The resulting filtered image $\mathbf{J}$ is an enhanced version of $\mathbf{R}$, that presents

less discontinuities and a significantly reduced noise level. Nevertheless, the JBU filter fails when edges in the original coloured image are lost after converting it to a grayscale image. We therefore propose to represent the 2-D image $\mathbf{I}$ using the proposed CA model instead. We hence need to replace d with a new distance d_{CA} between two values $\zeta_{\mathbf{p}} = \mathbf{I}(\mathbf{p})$ and $\zeta_{\mathbf{q}} = \mathbf{I}(\mathbf{q})$. We define d_{CA} as an approximation of the cylindrical distance d_{cyl} commonly used on the HCL space and defined as [5]:

$$d_{cyl}(\zeta_{\mathbf{p}}, \zeta_{\mathbf{q}}) = \sqrt{(\Delta l)^2 + (\Delta c)^2 + 4 \cdot c_{\mathbf{p}} \cdot c_{\mathbf{q}} \cdot \sin^2(\frac{\Delta h}{2})}, \quad (9)$$

where $c_{\mathbf{p}}$ and $c_{\mathbf{q}}$ are chrominance values correponding to $\zeta_{\mathbf{p}}$ and $\zeta_{\mathbf{q}}$, respectively. We simplify this distance for our model by considering a normalized value $\Delta\zeta$ instead of the first term Δl. The normalization factor a_1 is such that we achieve a total distance of one between the two reference colours black and white, where all the other terms become zero. Thus, we find $\mathsf{a}_1 = \frac{1}{\mathsf{K_L}(\mathsf{K_L}+1)(\pi+1)}$. In addition, we consider the L_1 norm, and define d_{CA} as:

$$d_{CA}(\zeta_{\mathbf{p}}, \zeta_{\mathbf{q}}) = \mathsf{a}_1 |\Delta\zeta| + |\Delta c| + 2 \cdot \sqrt{c_{\mathbf{p}} \cdot c_{\mathbf{q}}} \left| \sin(\frac{\Delta\zeta}{2}) \right| .$$

While the above expression is relatively complex, due to computing chrominance values from (8), it is a first step towards defining a better distance d_{CA}, and evaluating the CA model as presented in Section 5.

V. EXPERIMENTAL RESULTS

First, we perform a global evaluation of the CA model by testing 100 different coloured images of objects from the Amsterdam Library of Object Images (ALOI) [12]. These images are in the RGB space. We transform them to the proposed CA colour model by following the steps presented in Section II and Section III. Fig. 2 plots the root mean square error (RMSE) between the original RGB images and the recovered ones for K and $\mathsf{K_L}$ varying from 0 to 255. We see that the error drops whenever $\mathsf{K_L}$ is less than K, which means that a very sparse sampling of the luminance component can be sufficient for an accurate representation. Moreover, as soon as K reaches approximately 100, the error approaches zero. While this number may vary depending on the nature of the images, it clearly does not need to be set greater than 255, as the intensity of digital images falls between 0 and 255. We proceed by evaluating the performance of an extension of the JBU filter, the pixel weighted average strategy (PWAS) filter [13], when filtering considering grayscale or CA encoded images. We use data from the Middlebury stereo dataset [14]. Each selected scene is represented by a 2-D RGB image and the corresponding depth map. We downsample the original depth maps by a factor of 8 in order to use them as low-resolution depth maps inputs ($\mathbf{R}$ in (9)), Fig. 3. After the filtering process, we compare the resulting enhanced depth maps with the original

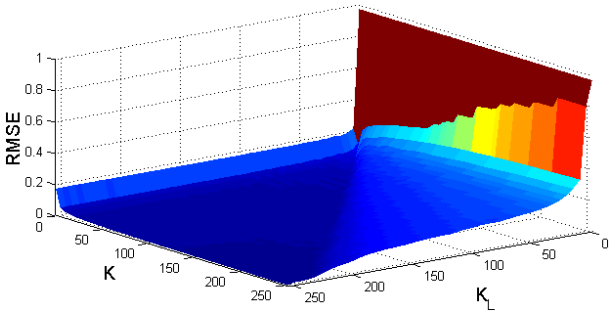

Fig. 2. RMSE between 100 images from the ALOI database and their CA transformed versions.

ones by using the structural similarity index (SSIM) [15]. Table I reports the computed SSIM values, where 1 means that the enhanced depth map perfectly coincides with the original one. Note that the PWAS filter always performs better when considering CA images. This significant improvement is well illustrated in Fig. 4 where we zoomed on a region from the Teddy scene. Fig. 4 also illustrates the enhanced depth map using the 2-D guidance image with different colour representations, similarly to experiments in [2]. Edge blurring and texture copying are clearly visible when considering a grayscale image (Fig. 4(d)). These artefacts are significantly reduced when filtering using RGB images, but colour bleeding is another artefact that remains due to filtering the 3 channels independently (Fig. 4(e)). If one filters all channels together (Fig. 4(f)), then some bleeding still occurs. Instead, filtering using an HCL image achieves satisfactory results (Fig. 4(g)), which are similar to those obtained from filtering using the proposed CA image (Fig. 4(h)).

Table I. SSIM comparison for the four scenes shown in Fig. 3 (1 corresponds to a perfect matching).

	Venus	Cones	Art	Barn
SSIM for Grayscale	0.974	0.835	0.837	0.948
SSIM for CA model	0.989	0.888	0.873	0.974

VI. CONCLUSION

We have presented a new colour model to overcome the limitations due to grayscale image filtering without modifying filtering algorithms. Indeed, the proposed cumulative angle model reduces the dimensionality of 3-D HCL representation to a unique dimension while preserving original perceptual properties. We derived the cumultive angle model by sampling the HCL cone in two dimensions using spirals. The two sampling rates are important parameters that need to be further investigated in order to evaluate the extent of the colour data compression rate. Finding a simple and discriminative distance for the proposed model is another open question important for real-time colour filtering.

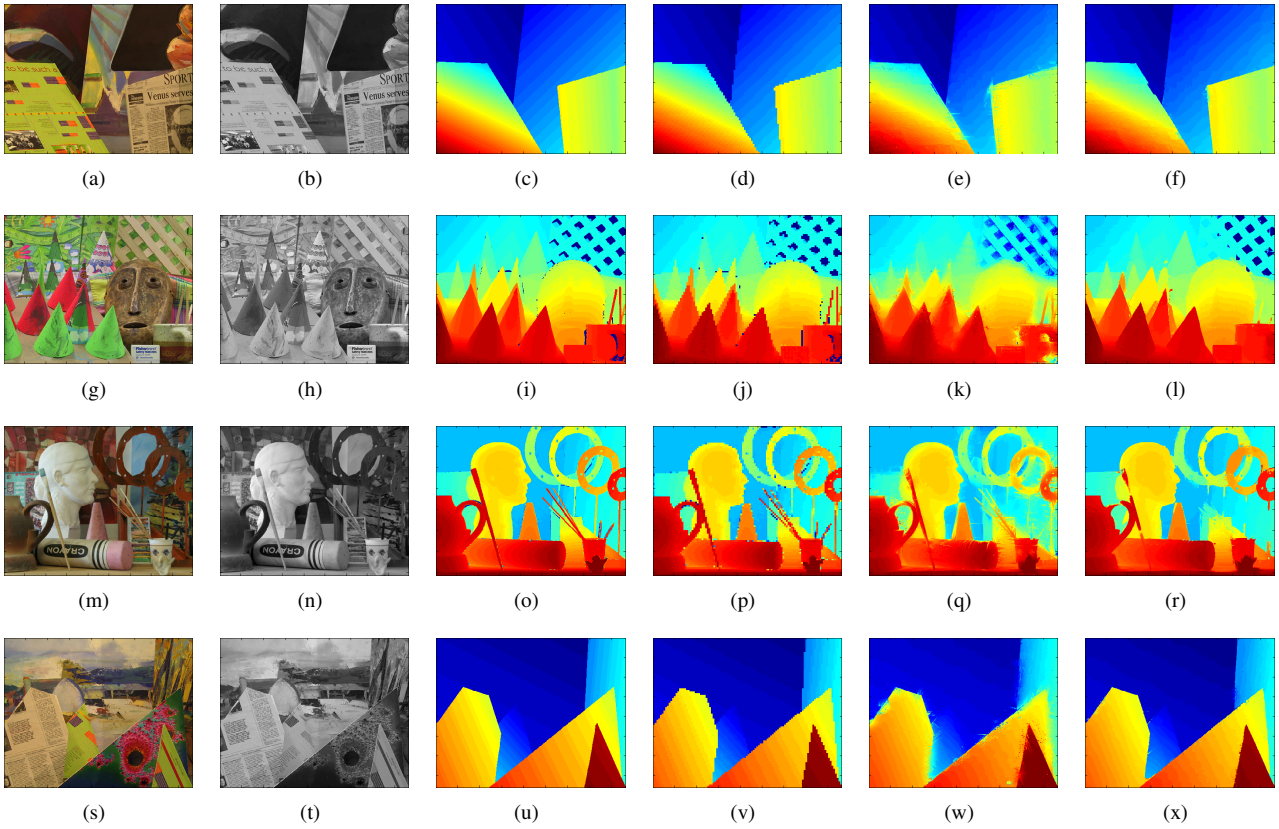

Fig. 3. Comparison between PWAS filtering considering grayscale and CA images. 1^{st} col.: RGB images. 2^{nd} col.: Grayscale images. 3^{rd} col.: Original depth maps. 4^{th} col.: Downsampled input depth maps. 5^{th} col.: Enhanced depth maps considering grayscale images ($\sigma_s = 10, \sigma_r = 0.02$). 6^{th} col.: Enhanced depth maps considering CA images ($\sigma_s = 10, \sigma_r = 0.1$). 1^{st} row: Venus scene. 2^{nd} row: Cones scene. 3^{rd} row: Art scene. 4^{th} row: Barn scene.

VII. REFERENCES

[1] J. Kopf, M. Cohen, D. Lischinski, and M. Uyttendaele, "Joint bilateral upsampling," in *ACM SIGGRAPH'07 papers*. New York, NY, USA: ACM, 2007, p. 96.

[2] S. Paris and F. Durand, "A Fast Approximation of the Bilateral Filter Using a Signal Processing Approach," in *International Journal of Computer Vision (IJCV)*, vol. 81,1. Kluwer Academic Publishers, 2009, pp. 24–52.

[3] T. Horiuchi, K. Watanabe, and S. Tominaga, "Adaptive Filtering for Color Image Sharpening and Denoising," in *14th International Conference on Image Analysis and Processing Workshops (ICIAPW)*, September 2007, pp. 196–201.

[4] X. Ding, X. Wang, and Q. Xiao, "Color image enhancement with a human visual system based adaptive filter," in *International Conference on Image Analysis and Signal Processing (IASP)*, April 2010, pp. 79–82.

[5] M. Sarifuddin and R. Missaoui, "A new perceptually uniform color space with associated color similarity measure for content based image and video retrieval," in *Proceedings of MIR'05 Workshop*, 2005, pp. 3–7.

[6] R. C. Gonzalez and R. E. Woods, *Digital Image Processing*, 2nd ed. Prentice Hall, 2002.

[7] G. Sharma and H. J. Trussell, "Digital Color Imaging," *IEEE TIP*, vol. 6, no. 7, pp. 901–932, 1997.

[8] J. Angulo, "Morphological colour operators in totally ordered lattices based on distances: Application to image filtering, enhancement and analysis," *in Computer Vision and Image Understanding*, vol. 107, no. 2–3, pp. 56–73, 2007.

[9] A. Vahdat and M. S. Drew, "Colour From Grey by Optimized Colour Ordering," in *Proceedings of CIC'10*.

[10] F. Garcia, D. Aouada, B. Mirbach, and B. Ottersten, "Spiral Colour Model: Reduction from 3-D to 2-D," in *International Conference on Acoustics, Speech and Signal Processing (ICASSP)*, vol. 10,6, 2011.

[11] E. H. Lockwood, *A Book of Curves*, 1st ed. Cambridge University Press, 1967.

[12] "Amsterdam library of object images," http://staff.science.uva.nl/aloi, May 2011.

[13] F. Garcia, B. Mirbach, B. Ottersten, F. Grandidier, and A. Cuesta, "Pixel Weighted Average Strategy for

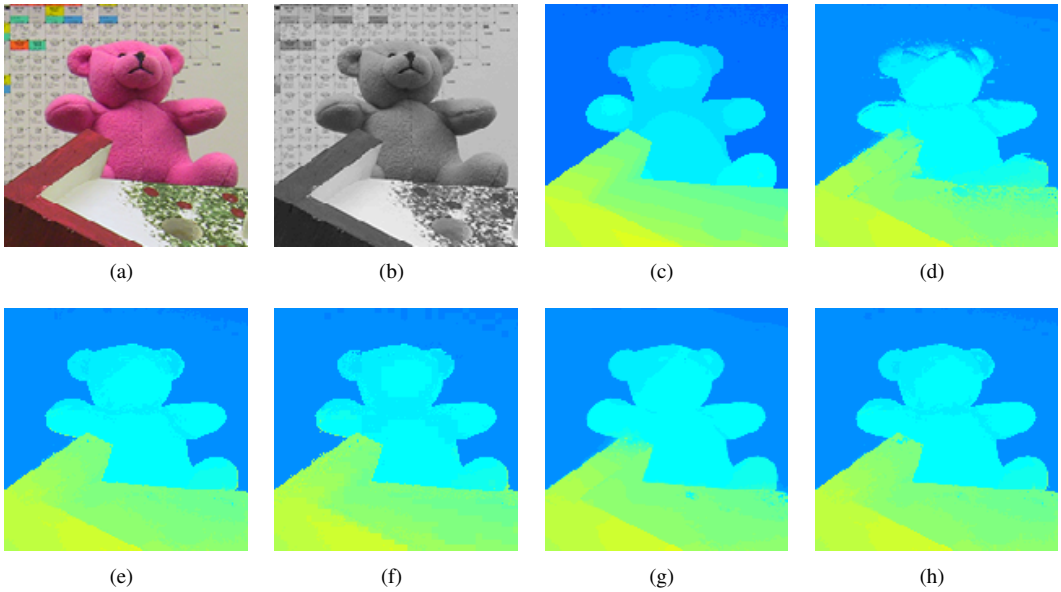

Fig. 4. Region from the Teddy scene. (a) RGB image. (b) Grayscale image. (c) Ground truth depth Map. (d) PWAS output using the grayscale image (b). (e) PWAS output using "per-channel RGB image" (a). (f) PWAS output using the RGB image (a). (g) PWAS output using the HCL image. (h) PWAS output using the CA image.

Depth Sensor Data Fusion," in *17th IEEE International Conference on Image Processing (ICIP)*, September 2010, pp. 2805–2808.

[14] "Middlebury stereo dataset," http://vision.middlebury.edu/stereo, May 2011.

[15] Z. Wang, A. C. Bovik, H. R. Sheikh, and E. P. Simoncelli, "Image quality assessment: From error visibility to structural similarity," in *IEEE TIP*, vol. 13-4, 2004.